URSI AP-RASC 2019, New Delhi, India, 09 - 15 March 2019

Statistical distribution of EMIC waves and dependence on substorm injections

B. Remya*(1), D. G. Sibeck(2), A. J. Halford(3), K. R. Murphy(2,4), G. D. Reeves(5), H. J. Singer(6), J. R. Wygant(7), G. Farinas Perez(8), S.A. Thaller(7), R. V. Reddy(1)
(1) Indian Institute of Geomagnetism, Navi Mumbai, India, Email:remyaphysics@gmail.com
(2) NASA Goddard Space Flight Center, Maryland, USA
(3) The Aerospace Corporation, Space Sciences Department, Chantilly, VA, USA
(4) Department of Astronomy, University of Maryland, College Park, MD, USA
(5) Los Alamos National Laboratory, Los Alamos, NM, USA
(6) NOAA Space Weather Prediction Center, Boulder, CO, USA
(7) School of Physics and Astronomy, University of Minnesota, Minneapolis, MN, USA
(8) University of Miami, Florida, USA

Abstract

The present study aims at understanding the distribution characteristics of electromagnetic ion cyclotron (EMIC) waves and also the role of ion injections in triggering EMIC waves in the Earth's magnetosphere. Van Allen Probes data is used to identify all EMIC wave events in the duration 2013-2015. The statistical dependence of EMIC wave events on L-shell, and MLT has been studied and compared with previous results. The role of substorm injections on EMIC wave occurrence is then studied in detail using one year EMIC wave event list. A comprehensive understanding of the individual substorm injected EMIC event and various parameters that affect wave triggering are illustrated using a case study of 09 August 2015 [also reported in Remya et al., 2018]. All these events are scrutinized based on the interplanetary conditions during individual event, geosynchronous measurements from the GOES and LANL and ground measurements. Night side (substorm) ion injections are shown to be able to provide favorable conditions for triggering EMIC waves in the absence of either a geomagnetic storm or a solar wind dynamic pressure event, which are believed to be the triggering mechanisms otherwise.

1. Introduction

Electromagnetic ion cyclotron (EMIC) waves are discrete electromagnetic emissions, typically in the frequency range of 0.1–5 Hz (Pc1 and Pc2 pulsations), which are believed to be generated by the ring current ions with temperature anisotropy ($T_{\perp} > T_{\parallel}$) [Cornwall, 1965]. They are excited with a left-handed and occur in bands categorized by the gyrofrequency of ions in the background plasma. This gyrofrequency distinction makes EMIC wave events to be categorized by bands: H+-band EMIC waves occurring between the proton and helium gyrofrequency, helium band waves occurring below the helium gyrofrequency and above oxygen ion gyrofrequency and oxygen-band EMIC waves occur below oxygen ion gyrofrequency. EMIC waves in their different bands have been observed and reported extensively [Min et al., 2012; Keika et al., 2013; Meredith et al., 2014; Saikin et al., 2015; Wang et al., 2015].

EMIC waves play a major role in Earth's magnetospheric dynamics. They contribute to the heavy ion heating by means of cyclotron resonance and also scatters protons in the ring current. They also pitch angle scatter relativistic electrons in the magnetosphere and contribute to particle loss in to the atmosphere. Hence the presence and generation of EMIC waves and their impact on energetic particle populations in the Earth's magnetosphere have drawn much attention in the near future space research. Understanding the distribution of these waves and their dependence on various geomagnetic conditions will give a better description of particle dynamics in the Earth's magnetosphere.

2. Data and methodology

Van Allen Probes (previously known as Radiation Belts Storm Probes - RBSP) orbiting below geosynchronous orbit throughout its span provides an unprecedented opportunity to characterize the statistical distribution of the EMIC waves in the inner magnetosphere. Three years (January 2013- December 2015) of data from the Electric and Magnetic Field Instrument Suite and Integrated Science (EMFISIS) magnetometer instrument on board the recently launched Van Allen Probes is utilized to carry out a detailed study on EMIC waves. An automated algorithm based on the Bortnik et al., 2007 technique is developed to detect the presence of EMIC waves. The algorithm uses the magnetic field data to plot the dynamic spectrum and records a wave activity if the wave power is higher than the background noise at least by one order of magnitude. The algorithm documents the basic information about each wave activity, like the wave frequency, local cyclotron frequency, start and end time of

the wave event, magnetic latitude (MLAT), magnetic local time (MLT) and L shell of occurrence, wave band (proton, helium or oxygen), and the geomagnetic indices like AE and SYMH during the event. A statistical survey of the EMIC wave occurrence pattern and distribution of EMIC waves in the different L-MLT sectors have been studied and compared with previous results.

3. Observations

3.1 Statistical results

Figure 1 shows an example of EMIC wave events found by the algorithm for both RBSP-A and RBSP-B on 27 February 2014 between 19:00 to 22:00 UT. The EMIC wave events are found to be excited in H and He band. It also looks like an O band wave is also present, however, since the O band frequency matches with the background noise, it is hard to differentiate between the wave and the noise. The white lines show the gyrofrequencies of proton (solid), helium (dashed) and oxygen (dotted). These EMIC events were found to be spread between L=4 and 5 and at local times between 13<MLT<14 hours. Both the probes were in close proximity (ΔL~0.35 and ΔMLT~0.3hrs) during their inbound orbit and observed the waves almost simultaneously.

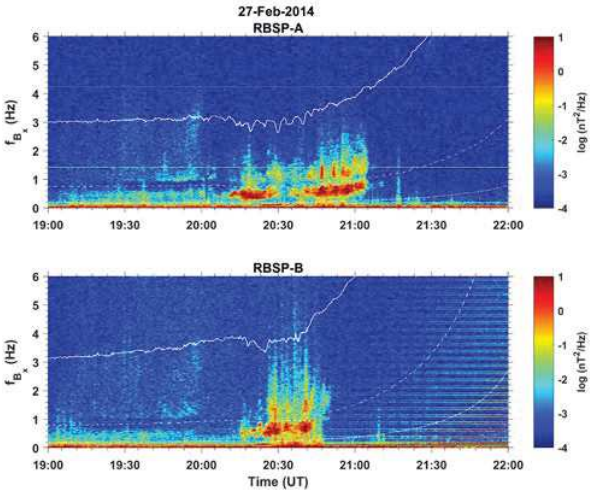

Figure 1. An example of EMIC wave events found by the algorithm between 19:00-22:00 UT on 27 February 2014 on both RBSP-A and B probes.

Figure 2 illustrates the combined dwell time of the Van Allen Probes A and B during 1 January 2013 to 31 December 2015. The bin size in the figure has 1 hour resolution in MLT and 1L resolution in L-shell. The unit of the color bar is hour. The L shell ranges between L=2 to L=7. Van Allen Probes have a very limited coverage beyond its apogee of 5.8 R_E and hence L>7 is not included. Figure 2 shows that the dwell time of the Van Allen Probes is > ~600 hours in all bins for 5<L<6. Higher dwell time in the night side at L>6 is due to the magnetic field stretching that the probes encounter at the night side. We further use this period to study the distribution characteristics of the EMIC waves.

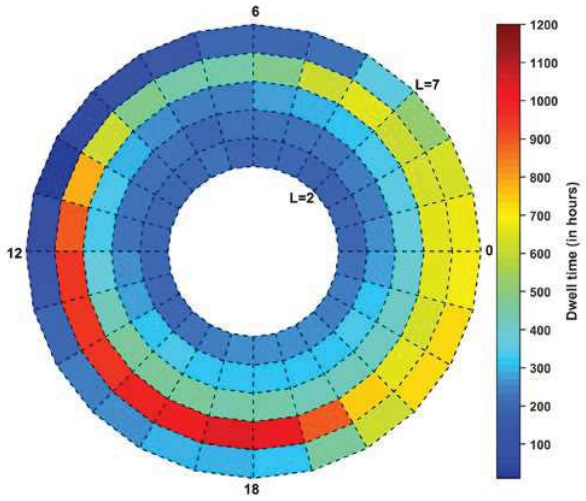

Figure 2. The data coverage of Van Allen Probes A and B from 01 January 2013 to 31 December 2015. The L shell ranges from L = 2 to L = 7 and each cell refers to 1 hour MLT by 1 L-shell. The unit for the color bar is hour.

A total of 1095 EMIC events which lasted at least 4 minutes in duration were detected using the automated algorithm. The distribution pattern in L-MLT is shown in Figure 3. The figure shows the occurrence rates for all EMIC wave activity observed by the Van Allen Probes over the three year study interval. The time duration of each EMIC wave packet has been catalogued and summed within each respective bin of MLT and L shell. The occurrence rate for each bin is then obtained as the total time EMIC wave is observed in a bin divided by the satellite dwell time in the respective bin. The time durations for both the probes have been added.

The peak occurrence rate is at the dusk sector between L=5 and 7 and 14<MLT<17 hours. Another peak is at lower L shells between L=3 and 5 and at local times near noon and between 17-19 MLT. This dusk sector peak is consistent with all the previous EMIC statistical results using AMPTE/CCE [Anderson et al., 1992], THEMIS [Min et al., 2012; Keika et al., 2013] and Van Allen Probes [Saikin et al., 2015; Wang et al., 2015]. Another peak occurs near the midnight sector with L between 3 to 4 and MLT between 00:00-02:00 UT. This was not found in previous studies using other satellites. Though Van Allen Probe studies suggest a similar peak, the L shell for the reported peaks were between L=5 and 6.

Each statistical study is different from another as they use different methods of wave detection, different satellites that cover different L shells and MLTs, and different time period of their study. Hence each study is statistically independent and yet important.

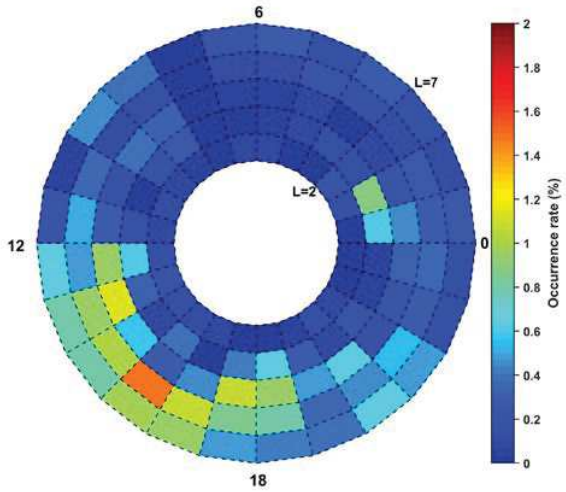

Figure 3. The occurrence rates of all EMIC waves observed by the Van Allen Probes from 1 January 2013 to 31 December 2015 from L=2 to L=7.

3.2 EMIC waves and substorm injections

It is understood that EMIC wave occurrence is favored during a geomagnetic storm and also during solar wind compressions of the dayside magnetosphere. However, the relation between EMIC wave occurrence and substorms have never been looked in detail, despite being the fact that substorms are much more frequent than geomagnetic storms. Using the database for EMIC waves for the year 2015, we study the events which were solely triggered due to substorm injections.

Out of a total 667 EMIC wave events in 2015, all the geomagnetic storm time and solar wind pressure pulse driven events were removed from the list. For the remaining 145 events, the interplanetary conditions, and magnetic field and particle data were analyzed in detail. The majority (86%) of these EMIC wave onsets were found to be associated with the arrival of ion injection signatures. The statistical distribution and occurrence pattern of these injection triggered EMIC wave events also suggest a peak occurrence at duskside (14-17 MLT) between 5<L<6 (not shown). The characteristic of such non-storm, non-pressure pulse driven EMIC event is illustrated using a case study of 09 August 2015 in one of our paper Remya et al., 2018. The event is discussed here in detail.

Figure 4 panel (a) shows the dynamic spectra for the EMIC wave event between 05:00-07:00 UT on 09 August 2015 observed by Van Allen Probe A. The satellite was at L~5.5 and ~18:00 MLT during the start of the EMIC wave activity. EMIC wave signatures are seen at frequencies in H band between proton and helium gyrofrequencies. Panels (b), (c) and (d) are the magnetic field components in spherical coordinates and the total magnetic field magnitude during the interval of study. It should be noted that the wave onset is associated with a dip in the magnetic field. This is due to the influx of the injected ions. RBSP-B was in its inbound trajectory at $L <$ 4, ~01:18 hr ahead of RBSP-A, and did not observe any EMIC wave activity during this period.

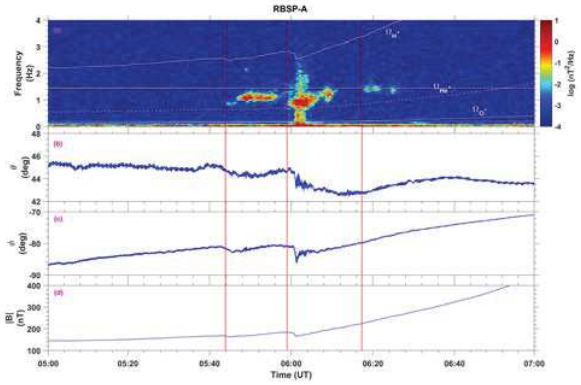

Figure 4. (a) The dynamic spectra of magnetic field observed by RBSP-A on 09 August 2015. (b–d) The time variation of the magnetic field components in spherical coordinates θ, ϕ, and magnitude of magnetic field $|B|$ as obtained from RBSP-A. The red vertical lines indicate the start time of each patch of the EMIC wave activity.

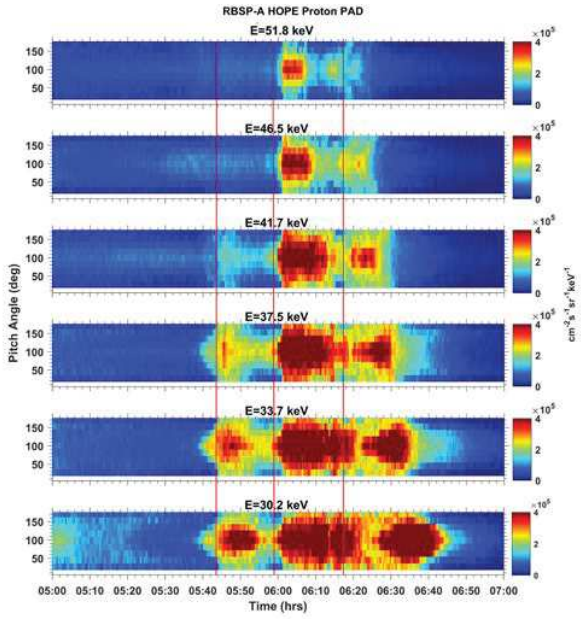

Figure 5. The pitch angle distributions (PADs) of 30.2- to 51.8-keV protons as observed by HOPE instrument on board RBSP-A. The energy decreases from top to bottom. Red vertical lines indicate the start time of each patch of the EMIC wave activity seen in Figure 4.

Figure 5 displays pitch angle distributions (PAD) for the top 6 proton energy channels (30.2 to 51.8 keV) observed by the HOPE instrument on board RBSP-A. The energy decreases from top to bottom as indicated on each panel. The red vertical lines match with the start time of the

EMIC wave patch as shown in the previous figure. Sudden increases seen in the proton flux at ~05:38 UT, ~05:56 UT, and ~06:11 UT indicate clear signatures of proton injection across all energies.

Proton injection signatures measured at GOES-15 are shown in Figure 6(a). GOES-15 observed sharp increases in proton fluxes at ~05:17 UT, ~05:38 UT and ~05:57 UT at all energies. Each of these flux rises show a double peaked behaviour. This suggests possible successive nightside injections. While the first injection signature was not seen by RBSP-A, the second and third injections seem to have reached RBSP-A almost simultaneously, which may have triggered the EMIC waves. GOES -15 was located at about ~20:00 MLT, close to the Van Allen Probe location.

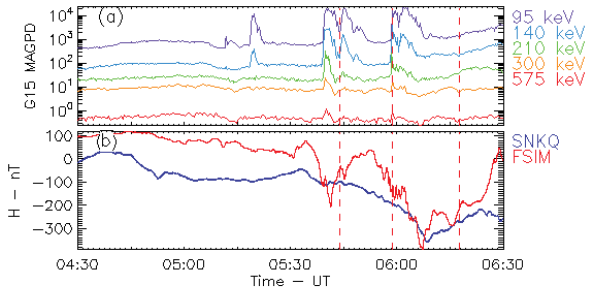

Figure 6. (a) The near-equatorial proton flux (in units of p/(cm^2 sr s keV) for 95- to 575-keV protons are plotted for GOES-15. (b) The magnetometer responses from two ground stations Sanikiluaq (SNKQ) (blue), conjugate to GOES-13, and Fort Simpson (FSIM) (red), conjugate to GOES-15.

Ground magnetic field measurements are shown in Figure 6(b) for two stations Sanikiluaq (SNKQ) (blue), conjugate to GOES-13, and Fort Simpson (FSIM) (red), conjugate to GOES-15. The plots indicate clear initiation of substorms at ~05:33 UT and another one at ~05:50 at FSIM characterized by a negative H-bay. These substorms are possibly associated with the non-dispersive flux rises observed at GOES-15. Associated injection signatures are also observed at the geosynchronous satellites LANL (See Figure 9 Remya et al., 2018).

Interplanetary conditions indicate an increase in AE index that starts from about 03:00 UT and exhibits two intensification to ~500 nT at ~04:48 UT and ~06:00 UT, and further increases to ~1,300 nT around 11:00 UT, much after the event (See Figure 1 Remya et al., 2018). All the EMIC events which were categorized as non-storm, non pressure pulse event were found to have associated injection signature.

4. Summary

This study shows global distribution characteristics of EMIC waves in all L-MLT sectors and also supports the role of substorm-injected ions for the growth of EMIC waves. the arrival of substorm ion injections produces magnetic field and plasma conditions that favour EMIC wave growth.

5. Acknowledgements

The Van Allen Probes EMFISIS data are available at http://emfisis.physics.uiowa.edu/, and HOPE data at https://rbsp-ect.lanl.gov/. The GOES satellite data are available at the website: https://satdat.ngdc.noaa.gov/sem/goes/data/. The solar wind parameters and geomagnetic indices are available at OMNI/CDAWeb: https://omniweb.gsfc.nasa.gov/. Portions of this research were funded by the Van Allen Probes mission.

6. References

1. Anderson, B. J., et al., A statistical study of Pc 1-2 magnetic pulsations in the equatorial magnetosphere: 1. Equatorial occurrence distributions, J. Geophys. Res., 97, 1992, doi:10.1029/91JA02706.

2. Bortnik, J., et al., An automatic wave detection algorithm applied to Pc1 pulsations, J. Geophys. Res., 112, A04204, 2007, doi:10.1029/2006JA011900.

3. Cornwall, J. M., Cyclotron instabilities and electromagnetic emission in the ultra low frequency and very low frequency ranges, J. Geophys. Res., 70(1), 1965, 61–69, doi:10.1029/JZ070i001p00061.

4. Keika, K. et al., Global characteristics of electromagnetic ion cyclotron waves: Occurrence rate and its storm dependence, J. Geophys. Res. Space Phys., 118, 2013, 4135–4150, doi:10.1002/jgra.50385.

5. Meredith, N. P. et al., Global morphology and spectral properties of EMIC waves derived from CRRES observations. J. Geophys. Res., 119, 2014, 5328–5342, doi:10.1002/2014JA020064.

6. Min, K., et al., Global distribution of EMIC waves derived from THEMIS observations, J. Geophys. Res., 117, A05219, 2012, doi:10.1029/2012JA017515.

7. Remya, B., et al., Ion injection triggered EMIC waves in the Earth's magnetosphere. J. Geophys. Res. Space Phys.,, 123, 2018, doi:10.1029/2018JA025354.

8. Saikin, A. A., et al, The occurrence and wave properties of H+-, He+-, and O+-band EMIC waves observed by the Van Allen Probes, J. Geophys. Res. Space Phys., 120, 2015, doi:10.1002/2015JA021358.

10. Wang, D., et al., Statistical characteristics of EMIC waves: Van Allen Probe observations, J. Geophys. Res. Space Phys., 120, 2015, doi:10.1002/2015JA021089.